Supplementary Information for

Promoting Low-Temperature Oxidative Dehydrogenation of Propane through Oxide–Support Interaction Regulation

Wenjie Li[1], Hong Wang[5], Zhandong Wang[1,5], Heng Cao[1,*], Jun Bao[1,2,3,4,*]

[1]National Synchrotron Radiation Laboratory, University of Science and Technology of China, Hefei, Anhui 230026, China.

[2]Key Laboratory of Precision and Intelligent Chemistry, University of Science and Technology of China, Hefei, Anhui 230026, China.

[3]*i*ChEM (Collaborative Innovation Center of Chemistry for Energy Materials), University of Science and Technology of China, Hefei, Anhui 230026, China.

[4]Anhui Industrial Innovation Research Institute of Advanced Optoelectronic Materials and Systems, Hefei, Anhui 230031, China.

[5]State Key Laboratory of Fire Science, University of Science and Technology of China, Hefei, Anhui 230026, China.

*e-mail: baoj@ustc.edu.cn; hengcao@ustc.edu.cn

Supplementary experimental section

Experimental procedures and analytical methods

The reaction was carried out in a vertical, 4-channel continuous-flow fixed-bed reactor (VDRT-200SMT, Quzhou Wode Technology Co. Ltd., CHN). Typically, a 200 mg sample of the NiO catalyst, diluted in quartz sand (40–60 mesh) to a total mass of 2 g, was loaded into a quartz reactor (inner diameter = 6 mm). The reaction carried out at 280–360 °C under atmospheric pressure, with a total gas flow rate of 40 ml/min and a feed gas composition of C_3H_8:O_2:Ar = 4:1:15. Two Agilent 8860 gas chromatographs were used for the analysis, one to analyze He, H_2, O_2, CH_4, CO and CO_2 using a thermal conductivity detector connected to a TDX-01 column and the other to analyze CH_4, C_2H_4, C_2H_6, C_3H_6 and C_3H_8 using a flame ionization detectors detector connected to a HP-Plot Q column. The calibration of gas concentration was conducted using standard gases, and helium was employed as an internal standard reference to account for the volume changes of the gas following the reaction. No C_2H_6 or CO was detected during the reaction. Conversions of C_3H_8 (X_{C3H8}) and O_2 (X_{O2}) were calculated according to equations (1) and (2). The selectivity of each carbon-containing product was evaluated on a molar carbon basis. For example, the selectivity of C_3H_6 was calculated from the relative concentrations in the outlet of carbon-containing product gas flow according to equations (3). The carbon balance (CB) in this work, calculated by equation (4), ranged between 97% and 102%.

$$X_{C3H8}(\%) = \frac{[C_3H_8]_{inlet} - [C_3H_8]_{outlet}}{[C_3H_8]_{inlet}} \times 100\#(1)$$

$$X_{O2}(\%) = \frac{[O_2]_{inlet} - [O_2]_{outlet}}{[O_2]_{inlet}} \times 100\#(2)$$

$$S_{C3H6}(\%) = \frac{[C_3H_6]_{outlet}}{[C_3H_6]_{outlet} + \frac{2}{3}[C_2H_4]_{outlet} + \frac{1}{3}[CH_4]_{outlet} + \frac{1}{3}[CO_2]_{outlet}} \times 100\#(3)$$

$$CB(\%) = \frac{[C_3H_8]_{outlet} + [C_3H_6]_{outlet} + \frac{2}{3}[C_2H_4]_{outlet} + \frac{1}{3}[CH_4]_{outlet} + \frac{1}{3}[CO_2]_{outlet}}{[C_3H_8]_{inlet}} \times 100\#(4)$$

where $[C_3H_8]_{inlet}$, $[O_2]_{inlet}$ are the concentration of C_3H_8 and O_2 in the feed stream of the inlet, respectively. $[C_3H_6]_{outlet}$, $[C_2H_4]_{outlet}$, $[CH_4]_{outlet}$ and $[CO_2]_{outlet}$ are the concentration of C_3H_6, C_2H_4, C_2H_4 and CO_2 in the feed stream of the outlet, respectively.

Characterization. X-ray diffraction (XRD) patterns were measured by SmartLab 9kW X-ray diffractometer (Rigaku Corporation, JPN) with Cu-Kα radiation (λ=1.54178 Å). Transmission electron microscopy (TEM), high-resolution transmission electron microscopy (HRTEM), high-angle annular dark-filed scanning transmission electron microscopy (HAADF–STEM), and energy dispersive X-ray (EDX) elemental mapping images were taken on a transmission electron microscope (JEM-2100Plus, JEOL, JPN) and a field emission high-resolution transmission electron microscope (JEM-F200, JEOL, JPN). X-ray photoelectron spectroscopy (XPS) measurements were conducted on ESCALAB 250Xi X-ray photoelectron spectrometer (Thermo Fisher Scientific, USA) with an Al Kα X-ray source (1486.6 eV) in Constant Analyzer Energy (CAE) mode with a pass energy of 30 eV for all spectra. The values of binding energies were calibrated with the C 1s peak of contaminant carbon at 284.8 eV. Inductively coupled plasma-atomic emission spectroscopy (iCAP 7400, Thermo Fisher Scientific, USA) was used to determine the loading of Ni species. Raman spectroscopy experiments were conducted at a Raman spectroscopy (LabRAM HR Evolution, HORIBA, FRA) with 473 nm laser excitation. sXAS spectra were obtained at the BL12B beamlines of the National Synchrotron Radiation Laboratory (NSRL) in Hefei. XAS spectra were obtained at the BL11B beamline of the Shanghai Synchrotron Radiation Facility (SSRF).

H_2-TPR. H_2 temperature-programmed reduction (H_2-TPR) experiments were conducted on an automatic chemisorption equipment (VDSorb-91i, Quzhou Wode Technology Co. Ltd., CHN). The NiO/SiO_2 catalysts were pretreated in a stream of Ar (30 ml/min) at 300 °C for 60 min. After cooling to room temperature in Ar, the gas flow was switched to 10% H_2/Ar (30 ml/min) and purged continuously until the baseline was stabilized. The temperature was then ramped to 800 °C at 10 °C/min, and the effluent gas signals were detected using a TCD detector.

C_3H_8 (C_3H_6-O_2) TPSR. C_3H_8 temperature-programmed surface reaction (C_3H_8-TPSR) experiments were conducted in a heating furnace, with the effluent gas analyzed by a reflection time-of-flight mass spectrometer (ProC-1, Jiangsu Puce Scientific Instrument Co. Ltd., CHN) equipped with a UV lamp. Prior to the TPSR measurement, the NiO/SiO_2 catalysts were pretreated in He stream (90 ml/min) at 300 °C for 60 min. After cooling to 50 °C in He, 10% C_3H_8/Ar (10

ml/min) was added and purged continuously until the baseline was stabilized. The temperature was then ramped to 600 °C at 10 °C/min. For the C_3H_6-O_2 TPSR experiments, the procedure was the same as the C_3H_8 TPSR, except the reaction gas was replaced with a mixture of 10% C_3H_6/Ar (10 ml/min) and O_2 (5 ml/min), and the final temperature was set to 400 °C.

In situ **DRIFTS.** *In situ* diffuse reflectance infrared Fourier transform spectroscopy (DRIFTS) experiment was carried out on a Nicolet iS50 (Thermo Fisher Scientific, USA) equipped with an MCT detector and a Harrick Praying operando cell. Spectra were collected in the range of 1000 to 4000 cm^{-1} with 64 scans at a resolution of 8 cm^{-1}. The NiO/SiO_2 catalysts were pretreated with Ar (40 ml/min) at 300°C for 30 min, after which the background spectrum was collected. Subsequently, the gas flow was switched to 5% C_3H_6/Ar (40 ml/min), and spectra were continuously recorded during the experiment. Once the adsorption of reactants reached saturation, the gas flow was switched back to Ar to eliminate interference of the gas-phase signals.

In situ **SVUV–PIMS.** *In situ* synchrotron vacuum ultraviolet photoionization mass spectrometry (SVUV–PIMS) experiment was carried out at the atomic and molecular physics beamline (BL09U) of the National Synchrotron Radiation Laboratory at Hefei, China. The molecular beam was introduced into the ionization chamber via the nozzle located at the center of the furnace, where it encountered synchrotron radiation light, leading to ionization. Subsequently, the ions were directed into the time-of-flight mass spectrometer for detailed analysis. A quartz catalytic reactor was connected to the SVUV–PIMS spectrometer, where the 100 mg NiO/SiO_2 catalysts (20–60 mesh) were loaded before the nozzle. During the ODHP reaction, the reaction gas, consisting of C_3H_8 (8 mL/min), O_2 (2 mL/min), and Ar (30 mL/min), was fed into the system. Once the mixture reached steady state, the temperature was increased to 400 °C at a rate of 10 °C/min. The effluent gas composition was then analyzed using the online SVUV–PIMS spectrometer. The photon energy was controlled at 11.2 eV, and the pressure was controlled at 780 Torr. To identify specific species, we changed the ionization energy from 8.9 eV to 11.2 eV at intervals of 0.1 eV during the ODHP reaction over NiO/SiO_2-CA at 400 °C.

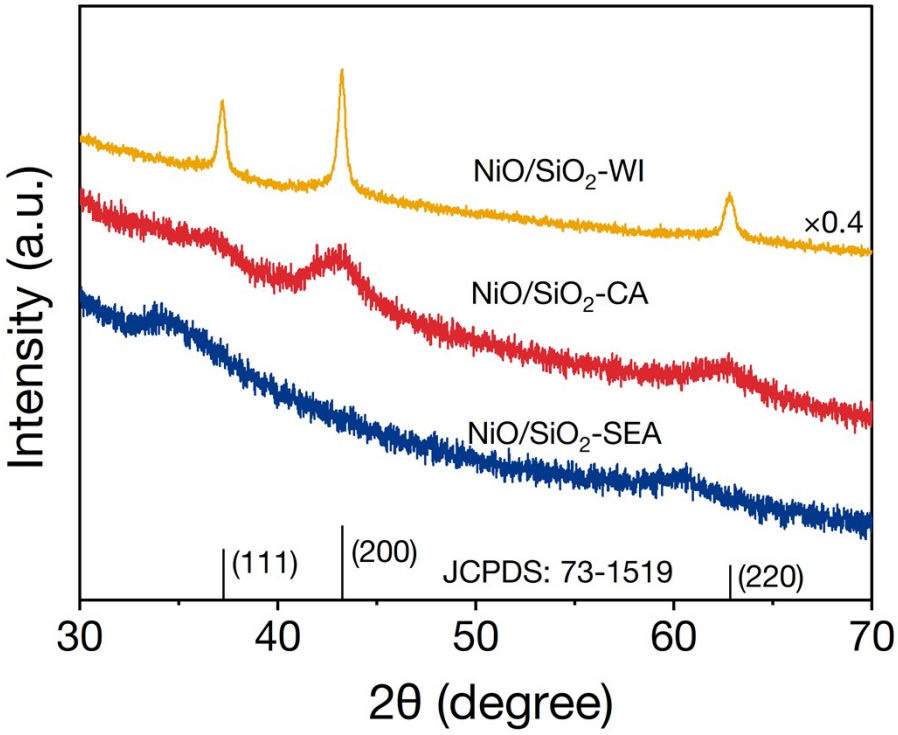

Figure S1. XRD patterns of NiO/SiO_2-WI, NiO/SiO_2-CA and NiO/SiO_2-SEA. To ensure clear visibility, the XRD result of NiO/SiO_2-WI was scaled down by a factor of 0.4.

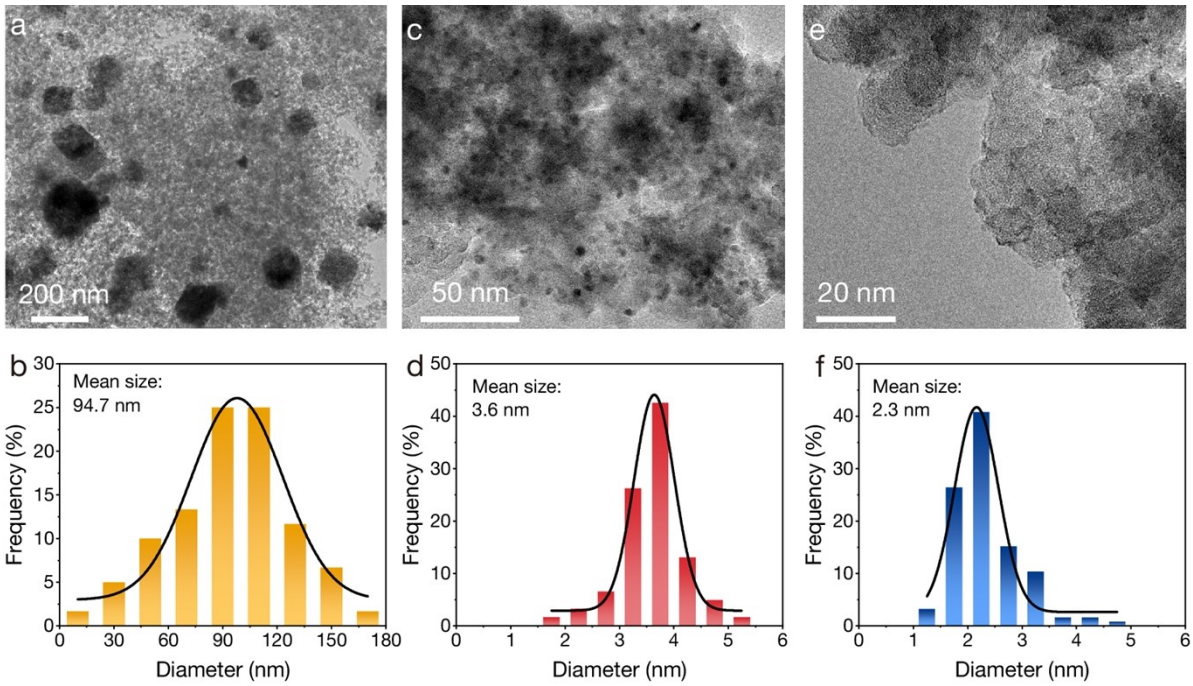

Figure S2. TEM images of (a) NiO/SiO_2-WI, (c) NiO/SiO_2-CA and (e) NiO/SiO_2-SEA, along with the corresponding nanoparticle size distribution histograms (b, d, f) determined by statistical analysis of more than 50 individual particles.

Supplementary Note 1.

Although the contrast between Ni and Si is subtle, the particles can be distinguished because SiO_2 is amorphous while NiO NPs are crystalline.

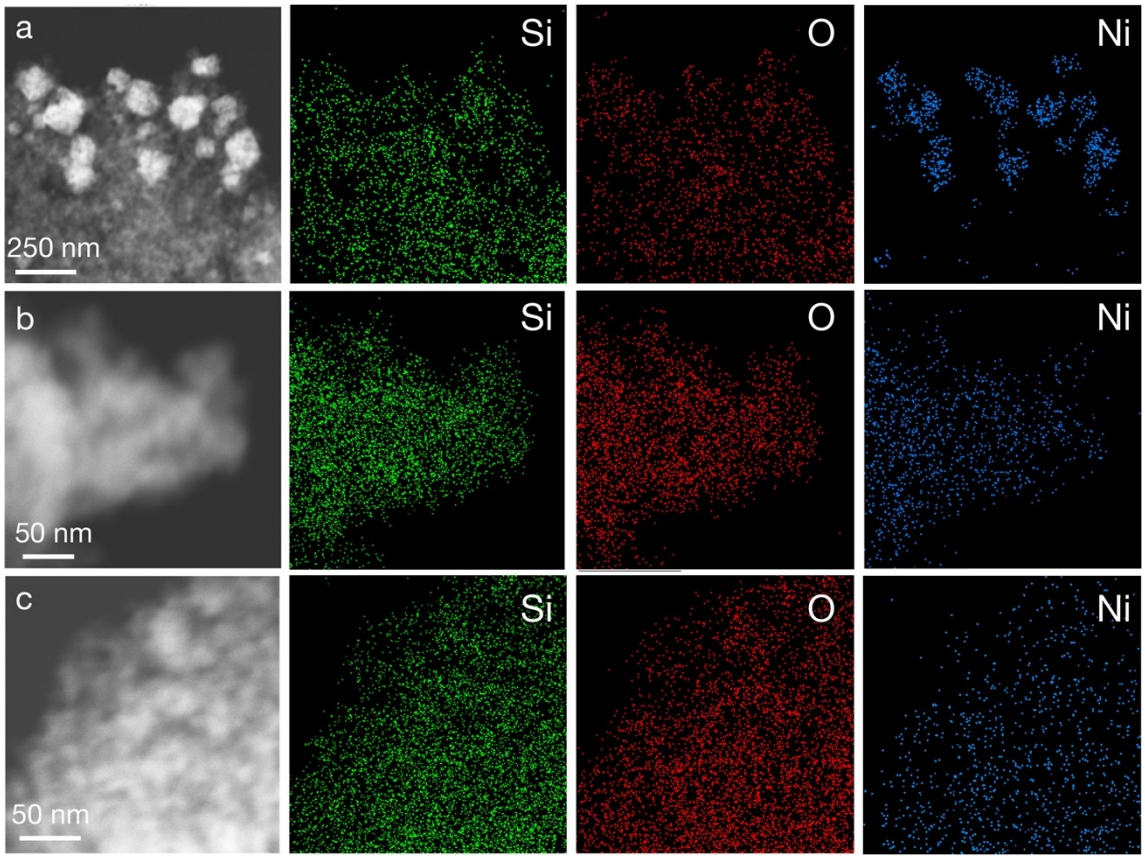

Figure S3. HAADF–STEM and corresponding EDX elemental mapping images of (a) NiO/SiO_2-WI, (b) NiO/SiO_2-CA, and (c) NiO/SiO_2-SEA.

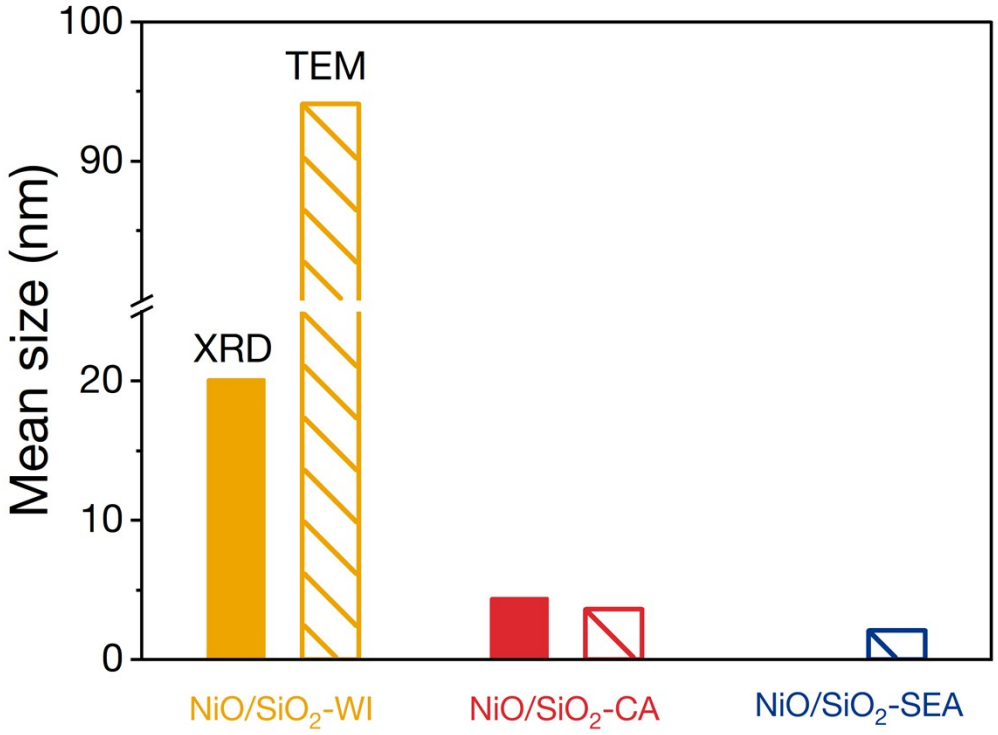

Figure S4. Mean particle sizes of NiO/SiO_2 catalysts determined by XRD (solid shadow column) and TEM (twill stripes column).

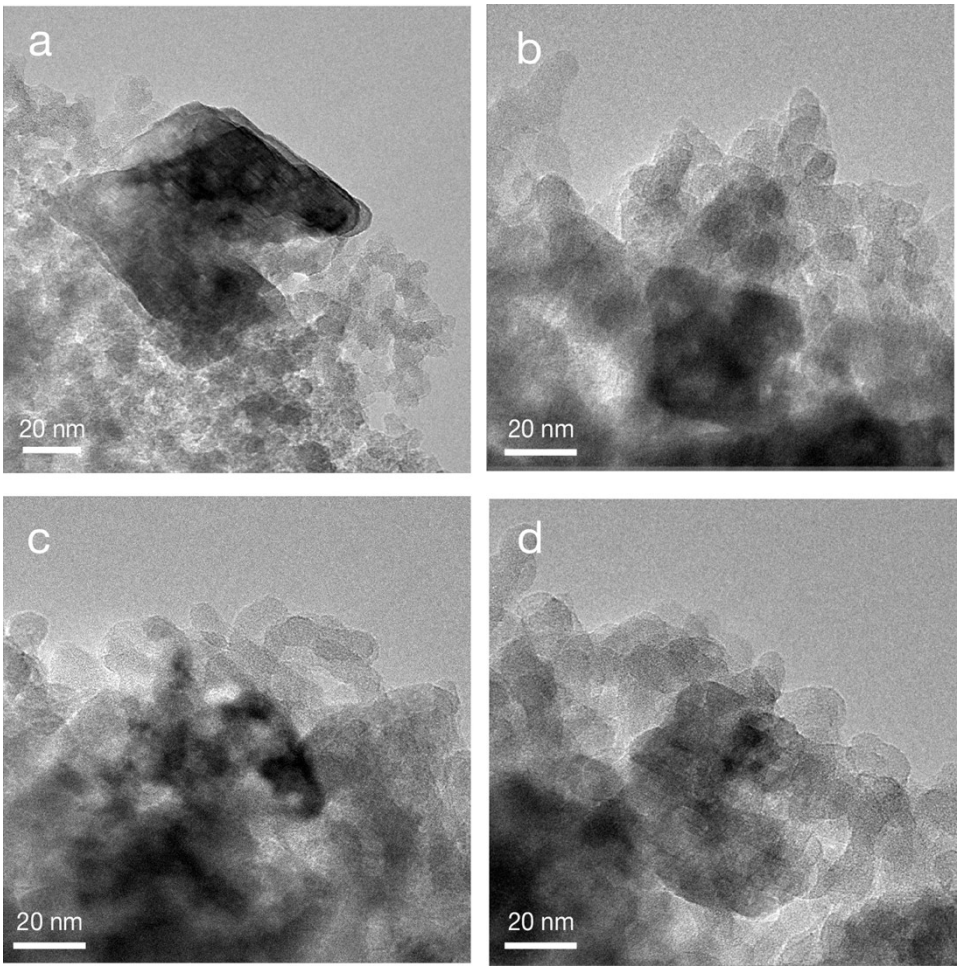

Figure S5. TEM images for NiO/SiO_2-WI.

Supplementary Note 2.

The SiO_2 edges were very smooth, with no prominent NiO NPs observed. Due to the weak OSI, NiO partially detached from the SiO_2 and underwent severe sintering, resulting in particle sizes larger than those of the SiO_2 support.

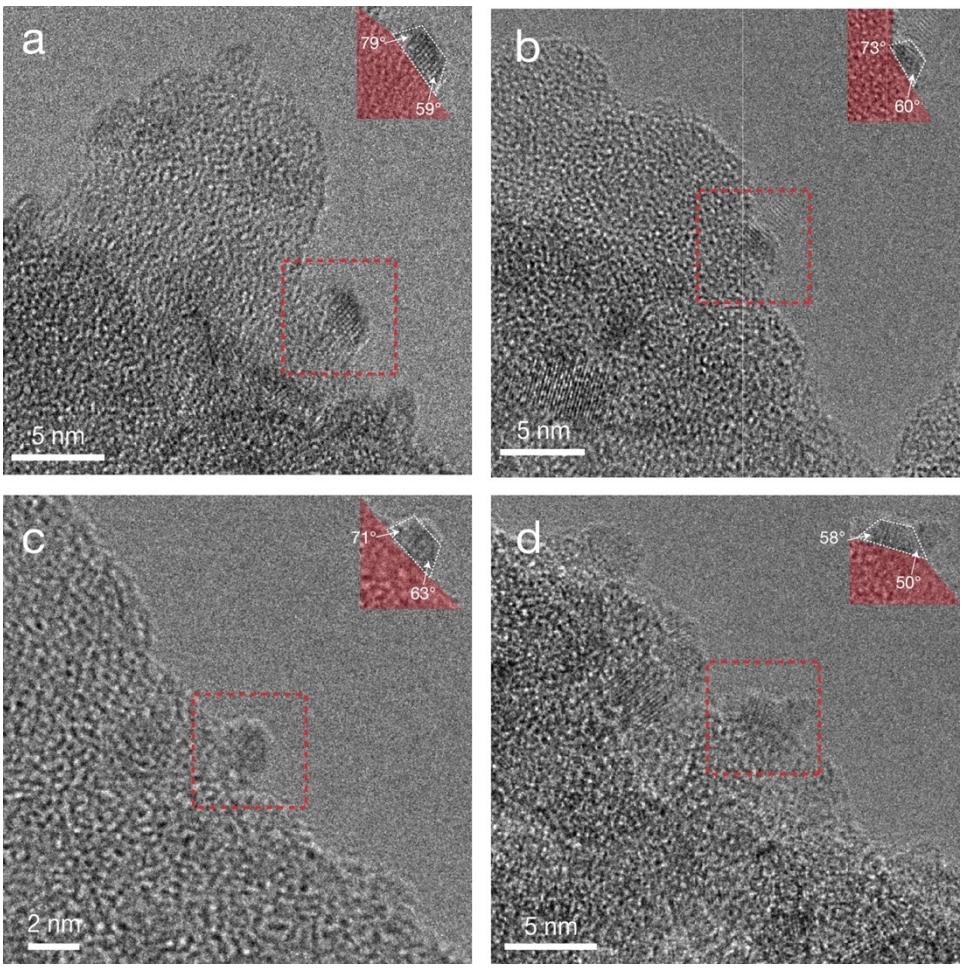

Figure S6. HRTEM images and the measured contact angle for NiO/SiO_2-CA.

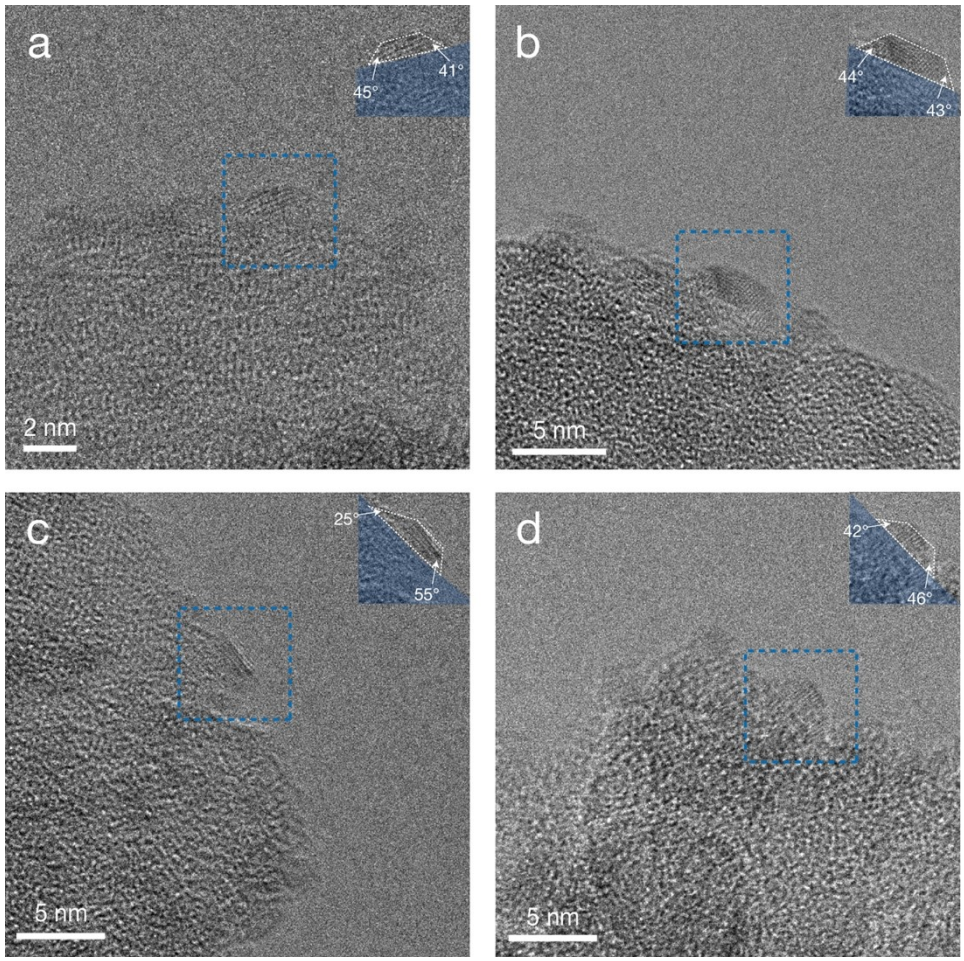

Figure S7. HRTEM images and the measured contact angle for NiO/SiO_2-SEA.

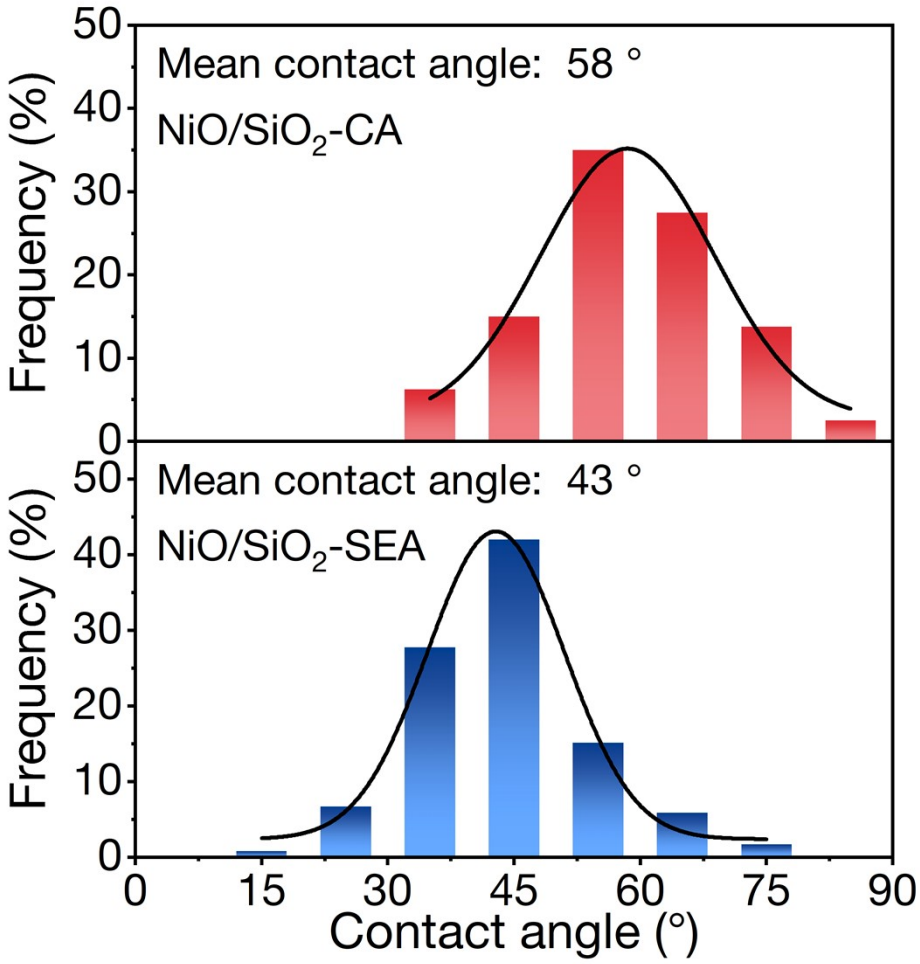

Figure S8. The distribution of contact angle between NiO NPs and SiO_2 support for NiO/SiO_2-CA and NiO/SiO_2-SEA, respectively.

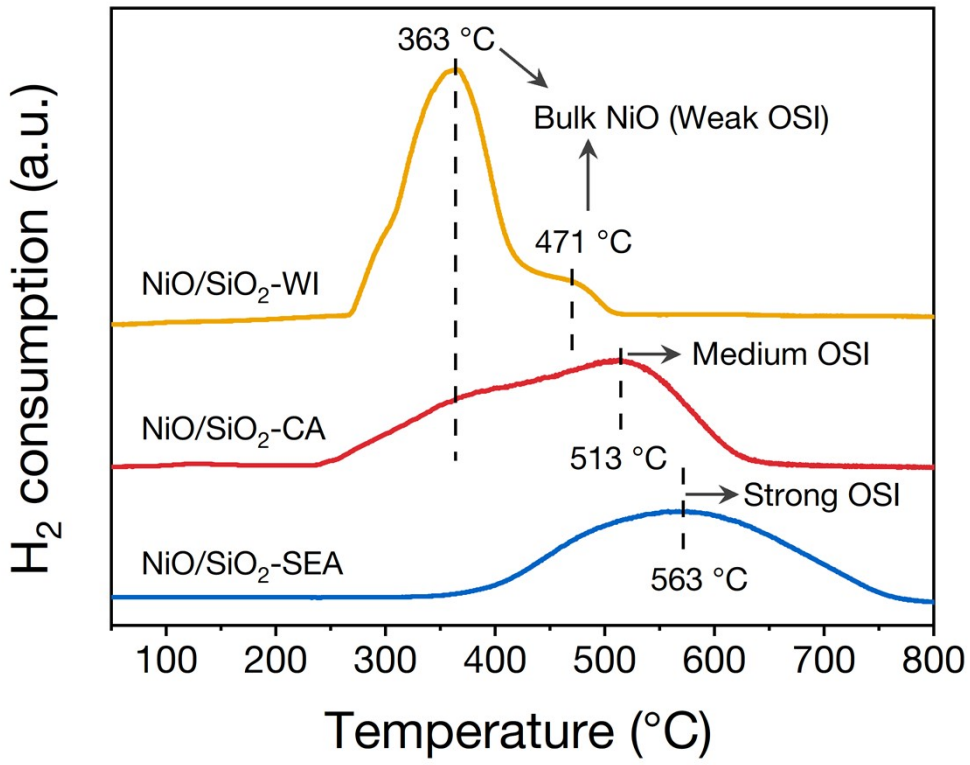

Figure S9. H_2-TPR profiles of the NiO/SiO_2 catalysts.

Supplementary Note 3.

The H_2-TPR profiles systematically reflect the evolution of OSI strength across the catalysts. For NiO/SiO_2-WI, the reduction peak centered on 363 °C contains a shoulder, assigned to the stepwise reduction of bulk NiO NPs ($NiO \rightarrow Ni^{\delta+} \rightarrow Ni^0$), indicative of a weak OSI. For NiO/SiO_2-CA, a new reduction peak appeared at 513 °C, which was attributed to the reduction of NiO at the interface between NiO NPs and SiO_2 support, reflecting a medium OSI.[1] For NiO/SiO_2-SEA, this interfacial reduction peak shifted further to 538 °C while the bulk NiO reduction signal disappeared, demonstrating the strongest OSI among the series.

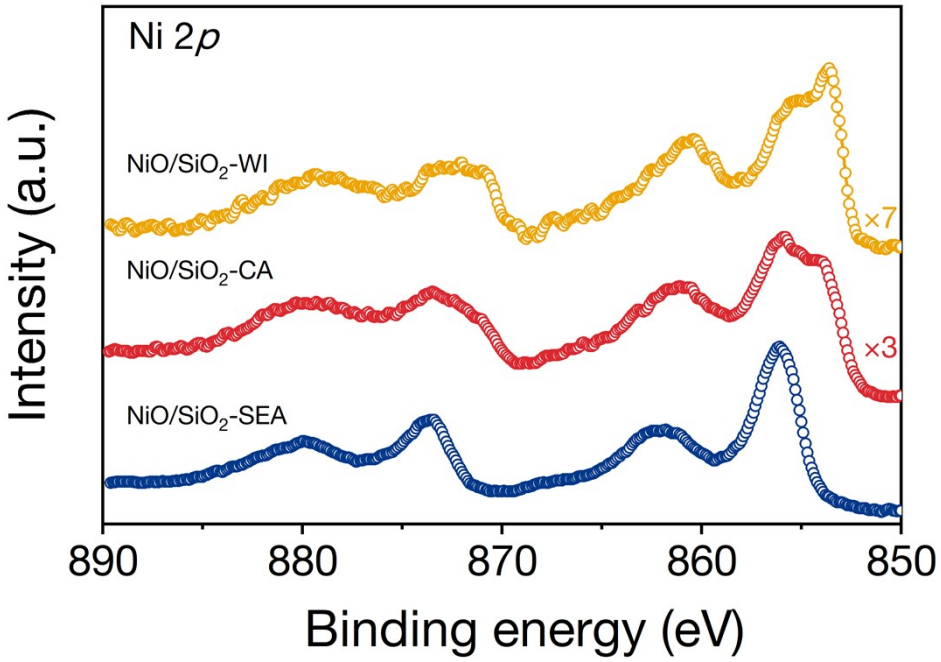

Figure S10. Ni 2*p* XPS results of the NiO/SiO_2 catalysts. For clear visibility, the XPS result of NiO/SiO_2-WI and NiO/SiO_2-CA was enlarged by 7 and 3 times, respectively.

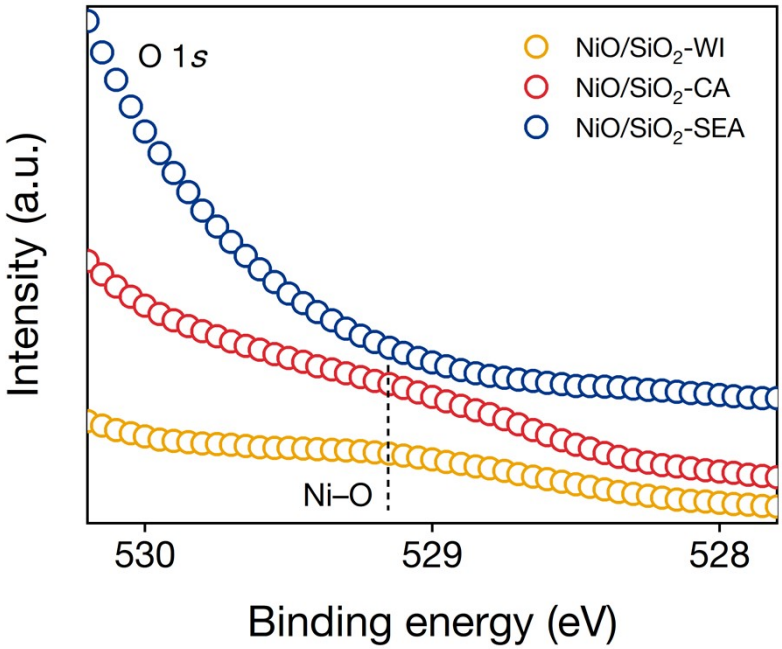

Figure S11. O 1*s* XPS spectra (528–530 eV) of the NiO/SiO_2 catalysts.

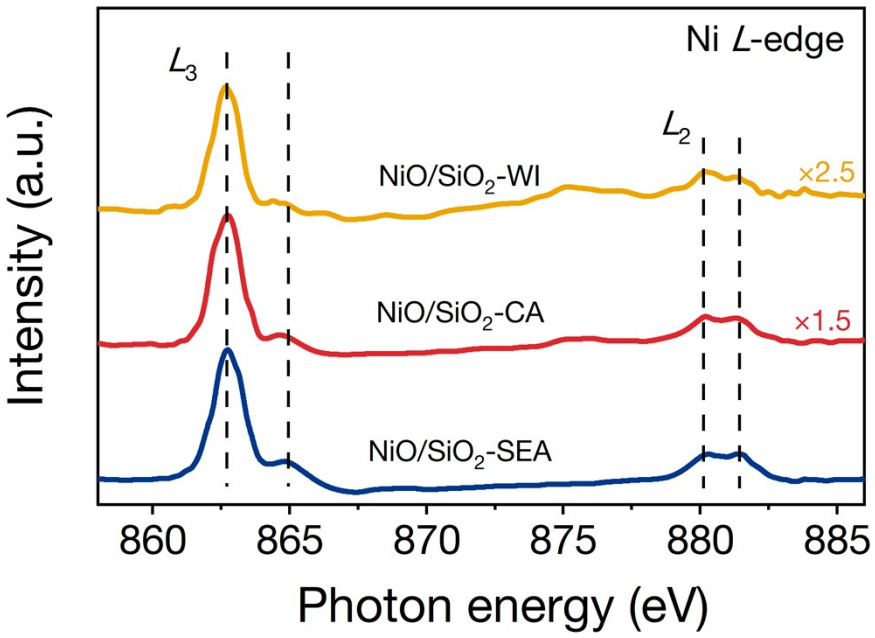

Figure S12. Ni *L* edge sXAS spectrum of the NiO/SiO_2 catalysts. For clear visibility, the sXAS result of NiO/SiO_2-WI and NiO/SiO_2-CA was enlarged by 2.5 and 1.5 times, respectively.

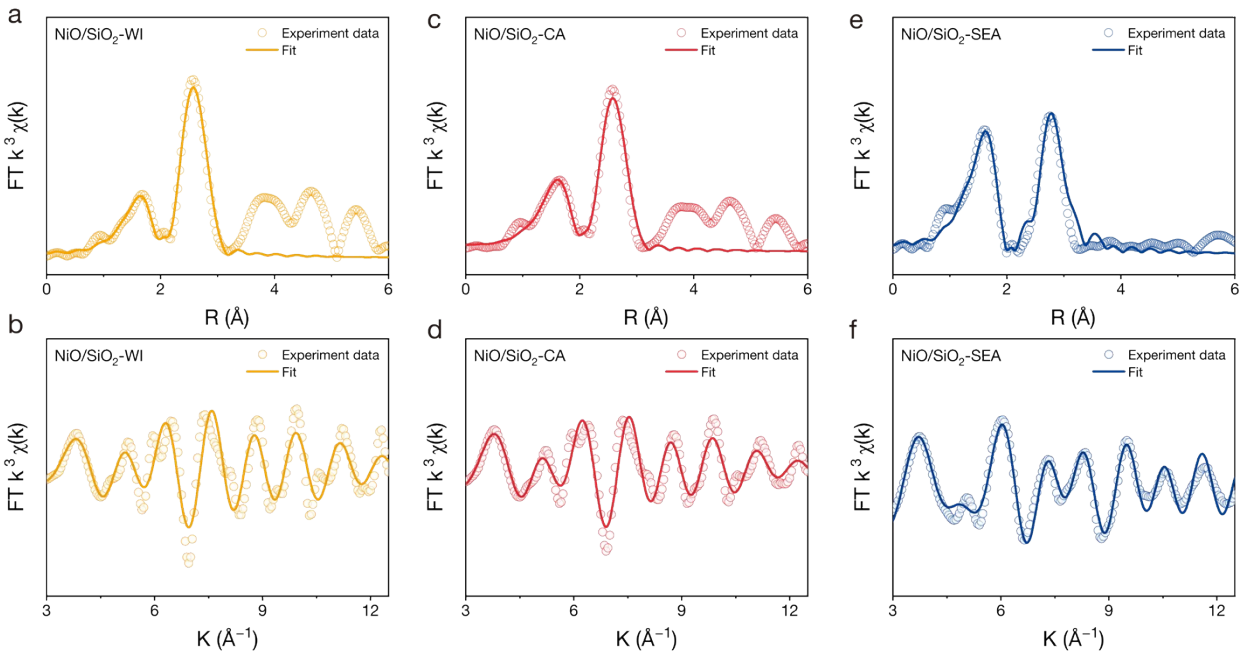

Figure S13. The Fourier-transformed EXAFS spectra at Ni *K* edge for (a, b) NiO/SiO_2-WI, (c, d) NiO/SiO_2-CA, and (e, f) NiO/SiO_2-SEA in (a, c, e) R space and (b, d, f) k space.

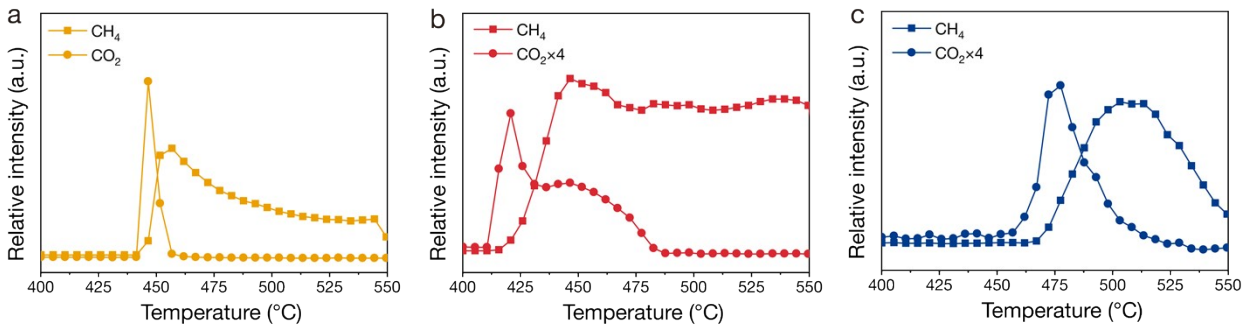

Figure S14. MS signals of CH_4 and CO_2 from C_3H_8 TPSR experiments for (a) NiO/SiO_2-WI, (b) NiO/SiO_2-CA, and (c) NiO/SiO_2-SEA. For clear visibility, the CO_2 intensity of NiO/SiO_2-CA and NiO/SiO_2-SEA was enlarged by 4 times.

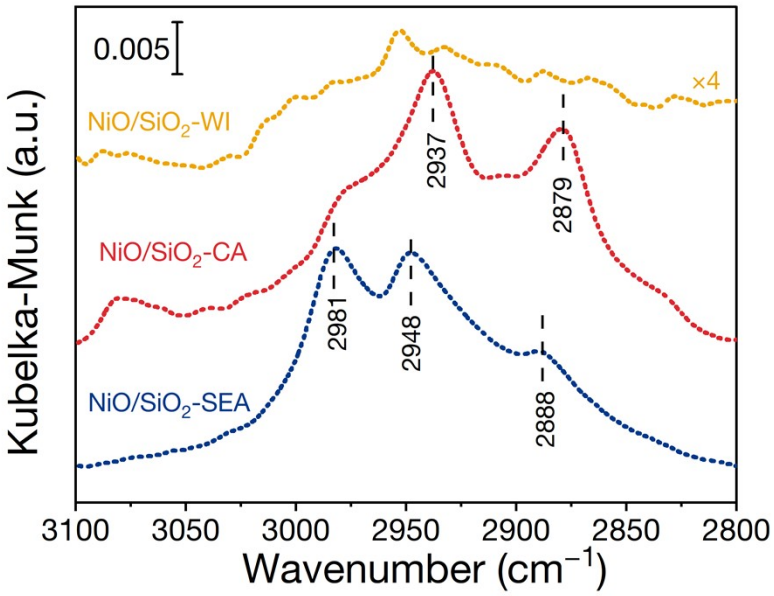

Figure S15. C_3H_6 DRIFTS spectra of NiO/SiO_2 catalysts range from 3100 to 2800 cm^{-1} at 300 °C. Dashed lines represent purge process. For clear visibility, the DRIFTS result of NiO/SiO_2-WI was enlarged by 4 times.

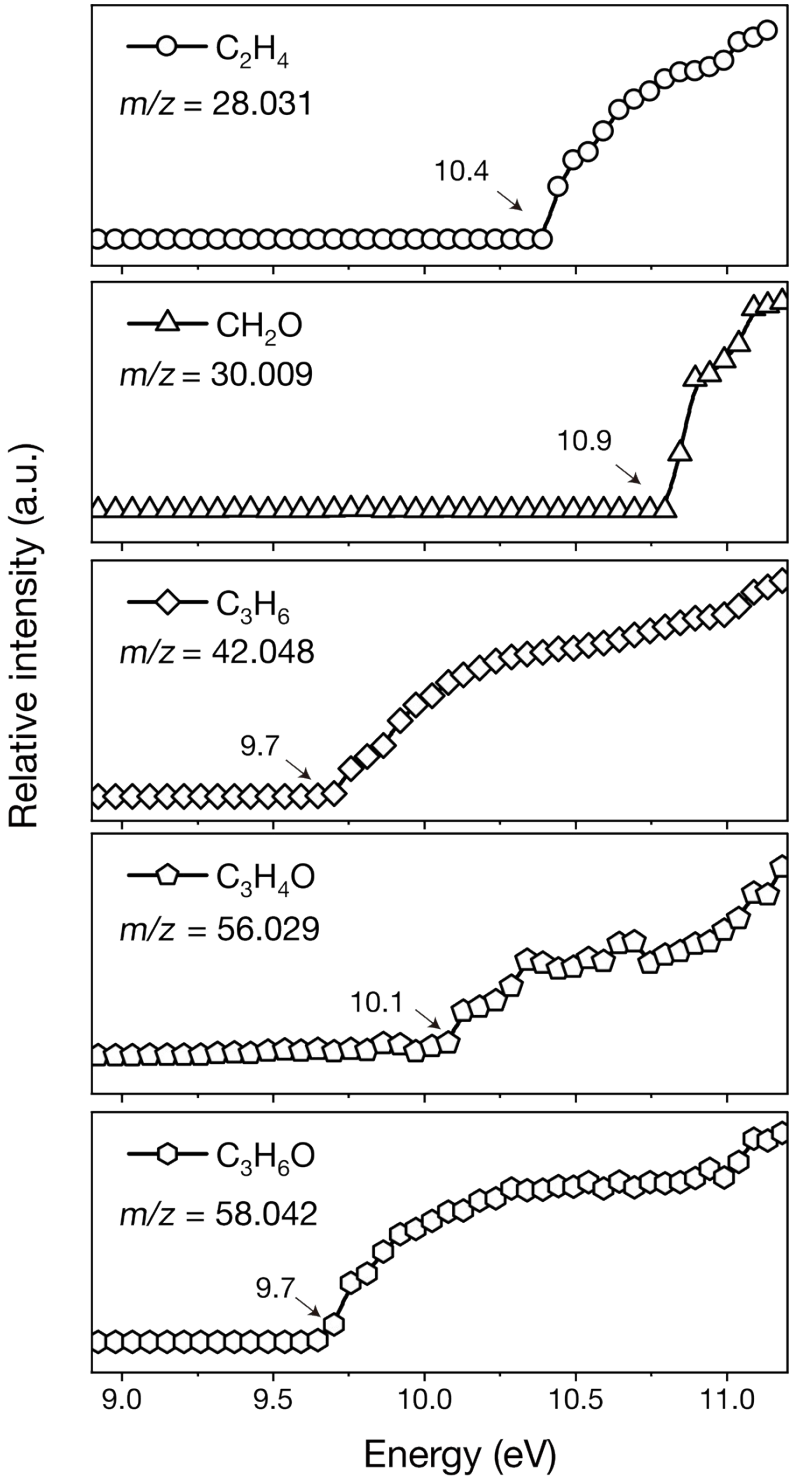

Figure S16. PIE curves of C_2H_4, CH_2O, C_3H_6, C_3H_4O and C_3H_6O.

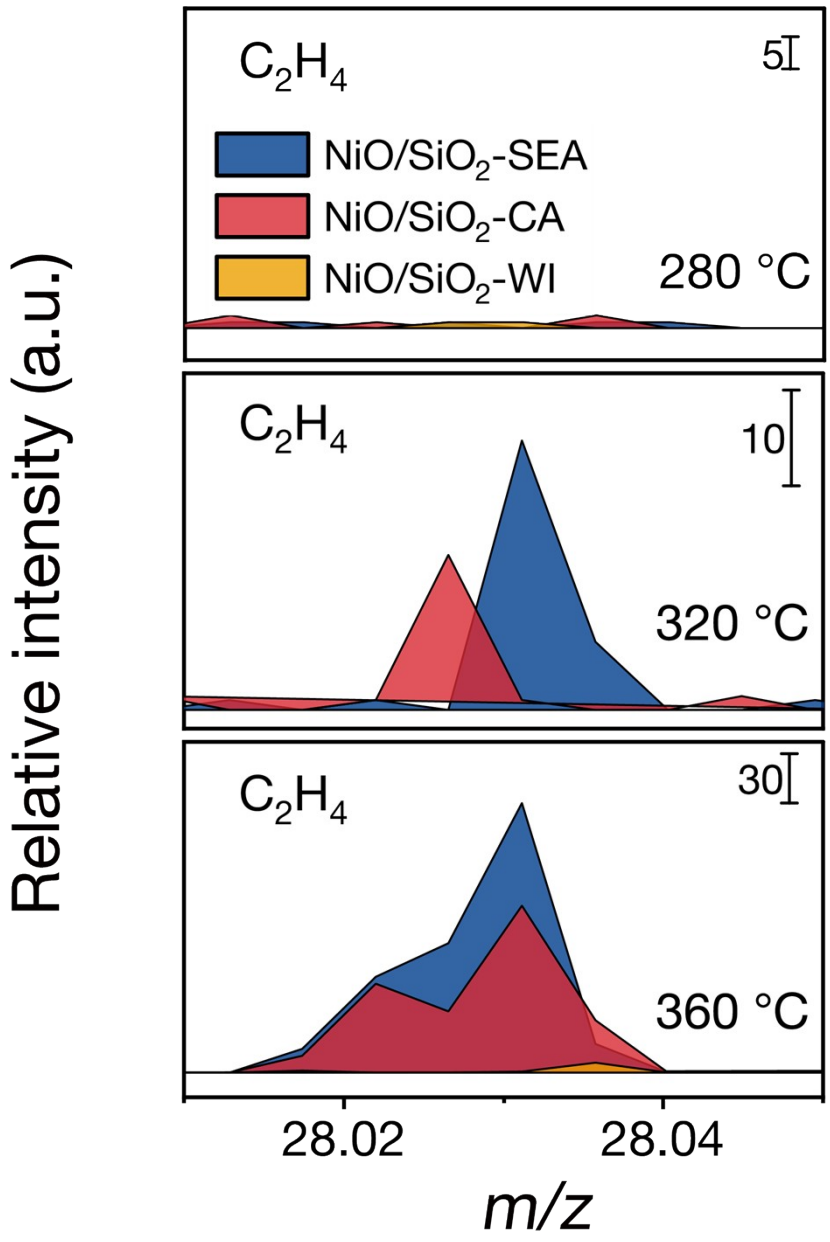

Figure S17. MS signals of the C_2H_4 from in situ SVUV–PIMS experiments during the ODHP at different temperatures for the NiO/SiO_2 catalysts.

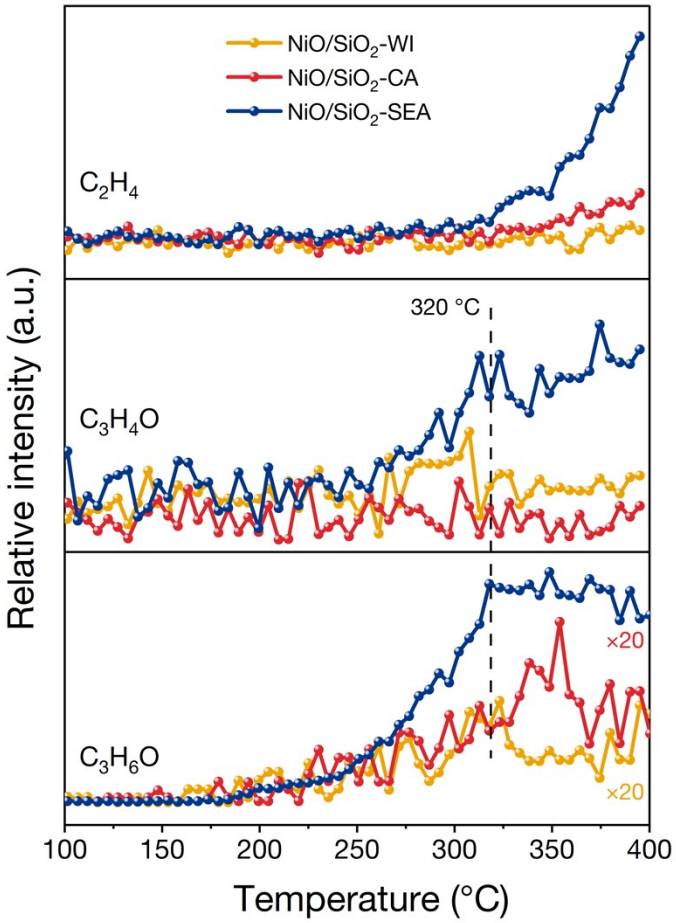

Figure S18. MS signals of the C_2H_4, C_3H_4O, and C_3H_6O from C_3H_6-O_2 TPSR experiments for the NiO/SiO_2 catalysts. For clear visibility, the C_3H_6O intensity of NiO/SiO_2-WI and NiO/SiO_2-CA was enlarged by 20 times.

Table S1 EXAFS fitting parameters at the Ni *K* edge of NiO and NiO/SiO_2 catalysts.

Sample	Shell	N^a	R (Å)[b]	σ^2 (Å^2)[c]	ΔE_0 (eV)[d]	r factor
NiO	Ni–O	6	2.074 (5)[e]	0.008	−3.08	0.008
	Ni–O–Ni	12	2.958 (8)	0.008		
NiO/SiO_2-WI	Ni–O	6.1 ± 0.9	2.075 (6)	0.008	−2.95	0.005
	Ni–O–Ni	12.2 ± 1.1	2.958 (8)	0.008		
NiO/SiO_2-CA	Ni–O	6.1 ± 0.8	2.072 (8)	0.009	−3.52	0.005
	Ni–O–Ni	10.7 ± 1.2	2.976 (6)	0.010		
NiO/SiO_2-SEA	Ni–O	5.3 ± 1.0	2.046 (11)	0.008	−5.33	0.017
	Ni–O–Si	4.7 ± 1.2	3.272 (13)	0.002		

[a] *N*, coordination numbers; [b] R, bond distance; [c] σ^2, Debye-Waller factors; [d] ΔE_0, inner potential shift; *r* factor was determined by the goodness of fitting. [e]2.074 (5) = 2.074 ± 0.0005. Amplitude reduction factor $S_0^2 = 1.15$ was obtained from fitting for the corresponding NiO, by fixing the *N* of Ni–O to 6 and Ni–O–Ni to 12.

Table S2. Summary of the ODHP performance of the NiO/SiO_2 catalysts shown in Figure 3.

Sample	T (°C)	Conversion (%)		Selectivity (%)				Reaction rate (mol mol_{Ni}^{-1} h^{-1})		
		C_3H_8	O_2	C_3H_6	CO_2	C_2H_4	CH_4	C_3H_8	C_3H_6	CO_2
NiO/SiO_2-WI	280	1.1	2.1	15.0	85.0	0	0	61	9	52
	300	1.3	2.4	21.0	79.0	0	0	69	15	55
	320	1.6	10.8	28.9	71.1	0	0	86	25	61
	340	2.5	27.5	32.6	67.4	0	0	140	46	95
	360	4.0	48.8	34.1	65.7	0.2	0	219	75	144
NiO/SiO_2-CA	280	3.3	17.9	63.9	36.1	0	0	176	112	64
	300	5.5	32.3	64.2	35.8	0	0	296	190	106
	320	7.8	54.4	62.7	37.2	0.1	0	418	262	156
	340	10.5	79.8	62.8	37.1	0.1	0	561	353	208
	360	12.9	97.4	62.6	37.1	0.2	0.1	692	433	257
NiO/SiO_2-SEA	280	0.8	2.2	40.3	59.7	0	0	44	18	26
	300	1.3	6.4	54.5	45.5	0	0	71	39	32
	320	1.9	9.9	57.8	41.7	0.5	0	102	59	42
	340	2.9	18.0	59.9	39.3	0.8	0	156	93	61
	360	4.4	32.4	59.5	39.1	1.2	0.2	237	141	93

Rerferences

1 D. Delgado, B. Solsona, A. Ykrelef, A. Rodríguez-Gómez, A. Caballero, E. Rodríguez-Aguado, E. Rodríguez-Castellón, J. M. López Nieto, *J. Phys. Chem. C* 2017, **121**, 25132–25142.